Electroless Deposition and Characterization of High Phosphorus Ni-P-Si$_3$N$_4$ Composite Coatings

J. N. Balaraju[*] *and K. S. Rajam*

Surface Engineering Division, National Aerospace Laboratories, Post Bag No. 1779, Bangalore 560 017, India
[*]E-mail: jnbalraj@css.nal.res.in

Composite coatings were prepared using hypophosphite reduced electroless nickel bath containing 1g/L submicron silicon nitride particles at pH 4.6 ± 0.2 and temperature 85 ± 2°C. Deposition rate was 6-8 µm/hour for both plain Ni-P and composite coatings. The amount of silicon nitride particles codeposited in the Ni-P matrix was around 3.5 wt.%. As-deposited coating surface composition analysis, carried out by Energy Dispersive Analysis of X-ray (EDX), results showed that plain Ni-P and Ni-P-Si$_3$N$_4$ deposits were having around 10 wt.% phosphorus. The X-ray diffraction (XRD) pattern of Ni-P-Si$_3$N$_4$ coating was very similar to that of plain electroless Ni-P coating in as-deposited condition. Presence of a single, broad peak around 45° 2θ which corresponds to Ni (111) peak was seen in both deposits. The calculated grain size by Debye-Scherrer method for both deposits was around 1.2 nm. Optical micrograph of the deposit cross-section revealed that the particles incorporation was uniform throughout the thickness of the coating. Phase transformation behavior studied by Differential Scanning Calorimeter (DSC) indicates that the particle incorporation had not influenced the crystallization temperature of the composite coatings. Presence of metastable phases like NiP$_2$ and Ni$_5$P$_4$ were observed for both coatings annealed at crystallization temperature. Increase in grain size of the deposits from 1.2 nm to 21 nm was also observed due to the annealing at crystallization temperature. Microhardness measurements made on the as-deposited and annealed (400°C) cross-sectional coatings showed that there was about 10% and 22% increase in hardness values respectively with the codeposition of silicon nitride particles.

1. INTRODUCTION

The ability to reinforce fine particulate matter such as hard ceramic or soft lubricious particles within metal matrix by electroless/autocatalytic plating method has lead to the development of composite coatings. These coatings exhibit superior properties compared to the plain electroless Ni-P

coatings. Composite coatings containing micron size second phase hard particles such as diamond, SiC, Al_2O_3, Si_3N_4, CeO_2, TiO_2 etc. and soft particles namely PTFE, MoS_2, HBN, graphite etc. have been successfully codeposited in Ni-P matrix [1]. These composite coatings find number of applications. For example the useful life of molds for plastics, rubber, etc., has been improved by coating them with Ni-P-SiC [2]. Electroless Ni-P-PTFE coatings offer non-stick, non-galling, high dry lubricity, low friction, precise and uniform torque and tension, good wear and corrosion resistance. The applications for these composite coatings have been in the fields include moulds for rubber and plastic components, tools for pumps, valves and butterfly valve for oil and gas industry, fasteners, precision instrument parts, aluminium air cylinders, carburetors, choke shafts, etc. [3]. Ni-P-diamond composite coatings are applied to improve the wear resistance of tools. Some examples are contact heads of honing heads, broaching tools for graphite, valves for viscous rubber masses and thread guides for use in textile machines and friction texturizing disks [4].

In general, electroless codeposition processes of second phase particle take place at low temperature and the chemical interaction is not favored between the particles and the matrix. The particles are only physically entrapped in the Ni-P matrix. Therefore heat treatment of these coatings is necessary in order to promote phase transitions which will influence their properties. Several investigators have successfully codeposited hard particles (like WC, SiC, TiO_2) in electroless Ni-P matrix [5-9]. Ni-P-WC (1 µm) composite coating was produced using an electroless nickel bath by varying the temperature and pH conditions [5]. It was concluded that phase structure cannot be varied by codeposition of WC particles in Ni–P alloy and it only influences the growth of crystal planes. The influence of vacuum heat treatment of electroless Ni-P-TiO_2 coatings on their structure and corrosion properties were discussed [6]. It was found that vacuum heat treatment (800°C) of the composite coatings could attain surface microhardness of 1500 HV with an excellent corrosion resistance. Electroless NiP micro- and nano-composite coatings containing SiC and Si_3N_4 particles were prepared and characterized for their structure and tribological properties [7]. Improved tribological properties were obtained with the annealed deposits containing particularly SiC particles. Formation of Ni_3Si phase was observed at high thermal treatments (500°C) for the Ni-P-SiC composite coating [8]. Medium phosphorus electroless nickel deposit containing micron size silicon nitride particles were prepared and characterized for their structure, corrosion and tribological behavior [9]. They have found that around 335°C phase transformation occurred for both plain Ni-P and composite coatings.

By scanning through the available literature on the composite coatings not much information is available on the phases formed and grain growth of the deposits at crystallization temperatures of high phosphorus electroless nickel composite coatings containing submicron silicon nitride particles. To prepare the composite coating the selection of second phase particles is also equally important. Silicon nitride is well known for its superior wear resistance, low coefficient of friction, higher hot hardness, good resistance to high temperature oxidation as well as to aqueous corrosion. Hence, systematic studies were carried out to prepare Ni-P-Si_3N_4 composite coatings by electroless deposition method. Plain Ni-P coatings were also prepared for comparison. Deposits were characterized for their structure, morphology, phase transformation behaviour and microhardness at various heat treatment temperatures. At crystallization temperatures deposits were heat treated and analysis was carried out to

find out the phases formed. Grain size has also been calculated for as-deposited and heat treated coatings at crystallization temperatures.

2. EXPERIMENTAL PART

Mild steel specimens (2.5 cm X 2.5 cm X 0.08 cm) were used for plating electroless nickel coatings. Specimens were ultrasonically cleaned in acetone, cathodically cleaned in 10% sodium hydroxide solution at 1A/ sq. inch for 5 minutes. Then specimens were thoroughly rinsed with deionized water and immersed in 50 vol.% sulphuric acid solution for deoxidization for 30 seconds. After deionized water rinse, specimens were transferred immediately to the plating solution.

Composition of the electroless nickel plating bath and its operating conditions were given in Table 1. The second phase particles used are Si_3N_4 (sub micron, ALDRICH make) particles. SEM image and XRD pattern of the submicron silicon nitride powder are shown in Figures 1 and 2 respectively. The characteristic peaks obtained for the silicon nitride particles from the XRD study were identified as that of α-silicon nitride. The deposition details have been described elsewhere [10]. The obtained deposition rate was in the order of 6 – 8 μms/hour. All the specimens were plated for 4 hours duration. For comparison plain electroless Ni-P samples were also prepared.

Table 1. Chemical composition of the electroless nickel plating bath and its operating conditions

| Chemical Composition	Concentration (g/L)
Nickel sulphate	21
Sodium hypophosphite	24
Lactic acid	25
Propionic acid	3
Lead acetate	3 ppm
Si_3N_4 (sub micron)	1
Operating conditions	
pH	4.6 ± 0.2
Temperature (°C)	85 ± 2
Magnetic stirring (rpm)	900 ± 25

For studying the surfaces and cross-sections of deposits, optical microscope (Leica make, Model DMIRM) was used, and the deposit composition was analyzed by SEM-EDX analysis. As-deposited cross-sectional deposits of both the coatings were etched in 10% chromic acid solution to find out the variation in phosphorus content.

The thickness of deposits was measured by weight gain method and also further confirmed by metallographic cross-sections of the deposits by optical microscope. Silicon nitride content (wt.%) present in the composite coatings was determined by dissolving the films in 1:1 nitric acid solution. Since silicon nitride particles were resistant to acid, it remains as such and hence, particles were centrifuged at 2000 rpm (Remi make). Acid solution was decanted and centrifuging was repeated thrice with deionized water so that particles were free from any metallic ions. Finally, wet particles

were dried in an oven at 100°C for more than 12 hours. By knowing the weights of the composite films and silicon nitride particles, percentage incorporation of silicon nitride was calculated.
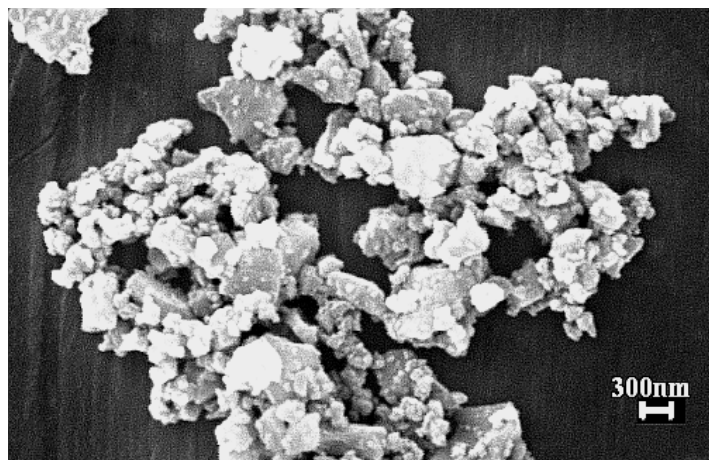
Figure 1. SEM image of agglomerated sub micron silicon nitride particles
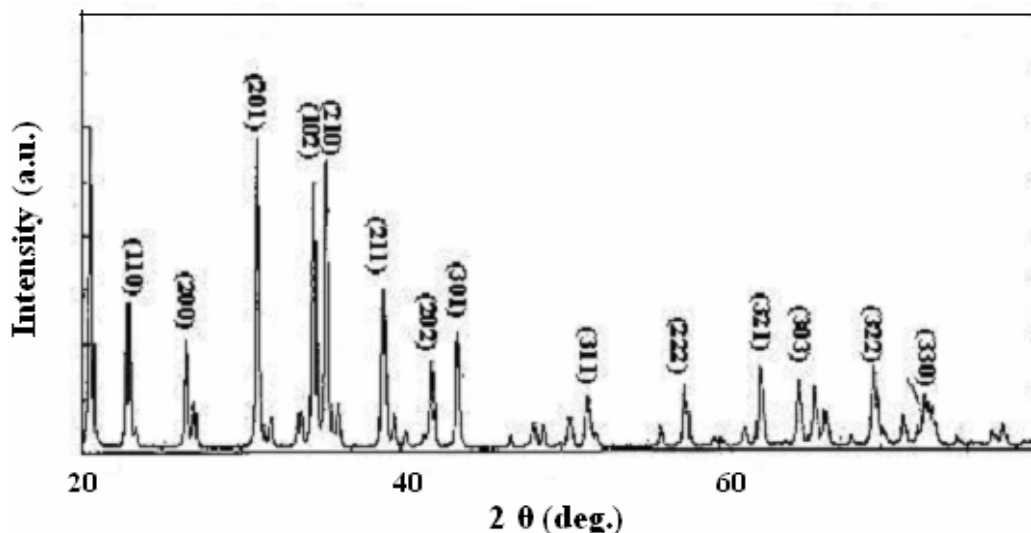
Figure 2. XRD pattern of sub micron silicon nitride particles

X-ray diffraction (XRD) analysis was performed with a Rigaku D/max 2200 powder diffractometer using Cu Kα radiation to study the structural changes in Ni-P-Si$_3$N$_4$ composite coatings.

For performing differential scanning calorimetric (DSC) analysis, the sample was taken in the form of a foil and cut into smaller pieces. About 50 mg sample was put in an aluminium pan and crimped using a cover. Empty aluminium pan with cover crimped was used as a reference. Continuous heating processes under different constant heating rates of 10, 20, 30 and 40°C/min. were performed in a Diamond DSC (Perkin Elmer model). The experiments were performed under continuous purging of the heating chamber with a nitrogen flow of 30 ml/ min. to avoid sample oxidation. The crimped sample specimen and reference were placed in a platinum furnace.

Microhardness measurements were also made on the cross-sections of the as-plated and heat-treated deposits (200, 400 and 600°C) of Ni-P and Ni-P-Si$_3$N$_4$ composite coatings using Buehler make

micro hardness tester with a Vickers diamond indenter (50-gf load). Five readings were taken on each deposit and the values were then averaged.

3. RESULTS AND DISCUSSION

3.1. Co-deposition of second phase particles

In the electroless nickel bath about 1 g/L submicron silicon nitride particles were added to obtain a Ni-P-Si$_3$N$_4$ composite coating. From the chemical analysis it was found that the second phase particle content codeposited in the Ni-P matrix was around 3.5 wt.%. The present electroless nickel bath was stable with only 1 g/L of second phase particle content. Beyond this it was observed that the bath got decomposed. In general, electroless nickel baths should be free from any contamination, impurities or foreign particles. Addition of second phase particles in the bath would lead to the bath decomposition. Hence, a more stable bath is required to obtain a composite coating containing insoluble second phase particles. In the present investigation electroless Ni-P-Si$_3$N$_4$ composite coatings were prepared by the bath containing 1 g/L silicon nitride particles with 3 ppm stabilizer. We have also observed that around 900 rpm is required to keep the second phase particles in suspension and to obtain uniform dispersion throughout the thickness of the deposit.

The co-deposition of particles is governed by a two step adsorption mechanism. In the first step the dispersed particles in the bath are transported to the surface of the electrode by mechanical action and are physically adsorbed due to the fluidal attack. In the second step these physically adsorbed particles dehydrate because of strong electric field of Helmholtz layer of the electrode, and a strong irreversible chemical adsorption of particles on the electrode takes place. The adsorbed particles are embedded by reduced metal or alloys. The physical adsorption is Langmiur adsorption, while the chemical adsorption is Temkin adsorption. The amount of physically adsorbed particle on the electrode is much larger than the chemically adsorbed one [11].

Several factors influence the incorporation of second phase particles in electroless nickel deposits. They include the size, shape and specific gravity of particles, particle charge, inertness of the particle, concentration of particles in the plating bath, method and degree of agitation, the deposition rate, compatibility of the particle with the matrix and the orientation of the part being plated [1, 12].

The incorporation of particles in the deposit during composite electroless plating greatly depends on size of the particle. In general, it is recommended that the particle must be large and heavy enough to settle in the solution, yet not as large as to cause the roughness of deposits or make it difficult for it to be held in suspension. In typical composite coatings, the fine particulate matter can be selected in the size range of 0.1μm to about 10μm, with a loading of up to about 40% by volume within the matrix. But it is suggested that the particle in the size range of 2-7 microns might be suitable for co-deposition in an electroless nickel matrix [1, 13]. Sarret et al have observed that when particle size in the range between 0.6 and 2 μm was used, the amount of embedded particles increased with particle size [7].

From the above it can be concluded that many factors affect the codeposition of second phase particles in electroless Ni-P matrix. Besides all these, bath chemistry and operating conditions should be optimized to get good incorporation of particles and hence to achieve required properties.

3.2. Coatings composition

Composition of the coatings, as determined by Energy Dispersive X-ray Analysis (EDX) is given in Table 2. Electroless plain Ni-P deposit is having a phosphorus content of about 10.6 wt.%. A marginal variation in phosphorus content can be seen due to the codeposition of submicron silicon nitride particles in Ni-P matrix. It shows that the second phase silicon nitride particles incorporation has not affected the phosphorus codeposition. Inclusion of alumina particles in high phosphorus Ni-P deposit has not affected the phosphorus content [10]. Where as Yucheng et al [14] have reported that the phosphorus content will be affected by the incorporation of micron size SiC particles. Slight decrease in phosphorus content has been observed when the super fine SiC particles incorporation in high phosphorus Ni-P matrix [15]. Similar observation was made in the case of nanometer size TiO_2 particle incorporation in high phosphorus Ni-P matrix [6].

Table 2. Composition of as-plated electroless nickel coatings determined by EDX

Type of deposited coating*	Phosphorus (wt.%)	Nickel (wt.%)
High Phosphorus Ni-P	10.6	89.4
High Phosphorus Ni-P- Si_3N_4	10.0	90.0

*Only Ni and P (100%) were considered.

3.3. Distribution of second phase particles

Optical images of surfaces and cross-sections of electroless Ni-P and Ni-P-Si_3N_4 coatings are shown in the Figures 3 (a-d). It is evident from the surface morphologies shown in the Figures 3 (a & c) that electroless plain Ni-P deposit surface is smoother and nodular free compared to that of composite coating with a nodular morphology with some porosity. Hence, it can be concluded that the inclusion of second phase particles in Ni-P matrix has resulted in nodular deposit. Similar observation has been made in the case of alumina particles codeposited in Ni-P matrix [10]. Whereas it has been reported that the incorporation of nano-sized particles modifies the growth of the NiP matrix to a larger extent than that of micro-sized ones, as surface morphology becomes nodular free with larger particles [7]. However, to further analyze the distribution of these particles through the thickness of the deposit, optical micrographs of the metallographic cross-section of the electroless composite coating has been prepared and is shown in the Figure 3(d). For comparison cross-section of the Ni-P coating is also shown in the Figure 3 (b). Figure 3(d) exhibits that the second phase particles are uniformly distributed throughout the thickness of the coating from the interface to the surface of the deposit. Particle agglomeration also can be seen in some places of the cross-section of the composite coating.
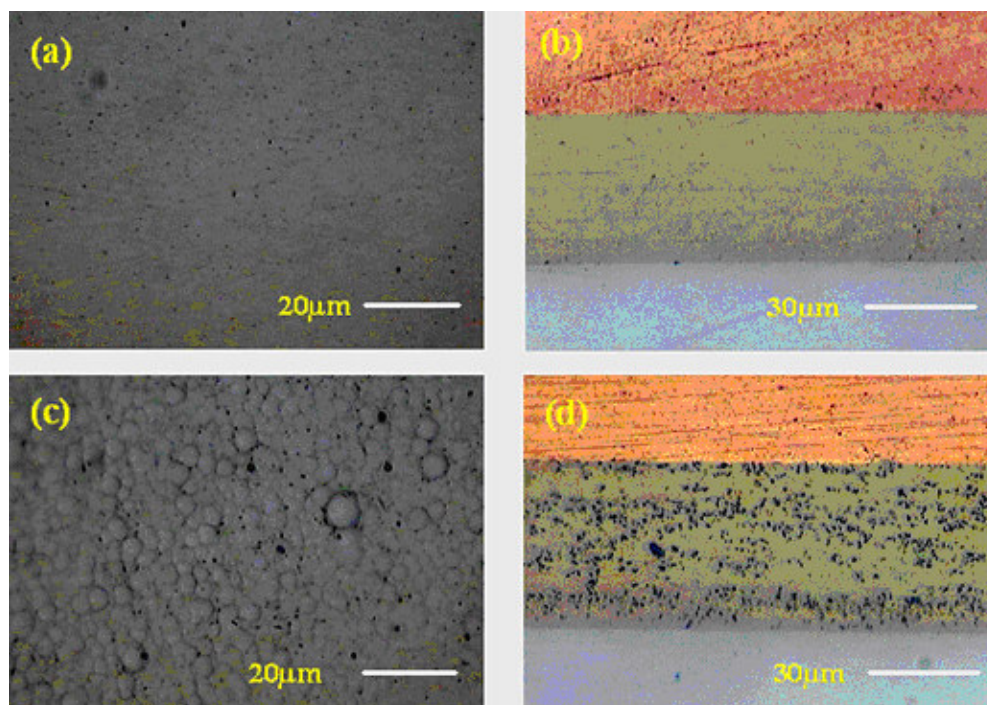
Figure 3. Optical micrographs of surfaces and cross-sections of as – deposited electroless Ni-P coatings (a & b) Ni-P; (c & d) Ni-P-Si$_3$N$_4$

3.4. Coatings structure

To determine the structure of the as-deposited coatings, X-ray diffraction (XRD) measurements are carried out using Cu K$_\alpha$ radiation. Diffraction pattern of high phosphorous Ni-P (Figure 4(a)) shows a single broad peak around 45° 2θ with preferred orientation of Ni (111) and the calculated grain size using Debye Scherrer method is around 1.2 nm. Theoretically a disorder in arrangement of atoms manifests itself as a broad peak in X-ray diffractograms. The observed diffractogram of the electroless Ni-P deposit can be explained based on the mechanism of formation of these deposits. As already stated, since phosphorous has lower solubility in nickel, it causes lattice disorder in the crystalline nickel. Higher the phosphorous in the coating, the higher will be the disorder and the structure becomes amorphous. Thus the system remains in the non-equilibrium amorphous state because of kinetic constraints and the low solubility of the phosphorus [16]. EDX analysis shows that the deposit contains about 10 wt.% P. Hence, it is evident that this higher phosphorus content has prevented the nucleation of f.c.c nickel phase and has resulted in an amorphous structure of Ni-P coatings.

The X-ray diffraction pattern of the electroless Ni-P-Si$_3$N$_4$ composite coating is shown in the Figure 4(b). It is evident that the X-ray diffraction pattern of the composite coating is similar to that of particle free coating. The calculated grain size from the Scherrer formula for the diffracted peak is about 1.4nm. Hence, it can be concluded that incorporation of Si$_3$N$_4$ particles in electroless Ni-P matrix has not influenced the structure of the composite coating. Similar observation has been made by Balaraju et al. [17]. Where as Yucheng et al [14] and Apachitei et al [18] have observed the SiC

reflection in the XRD pattern of as-plated electroless Ni-P-SiC composite coating. Probably it could be due to the higher amount of particles codeposition (around 7 wt.%).
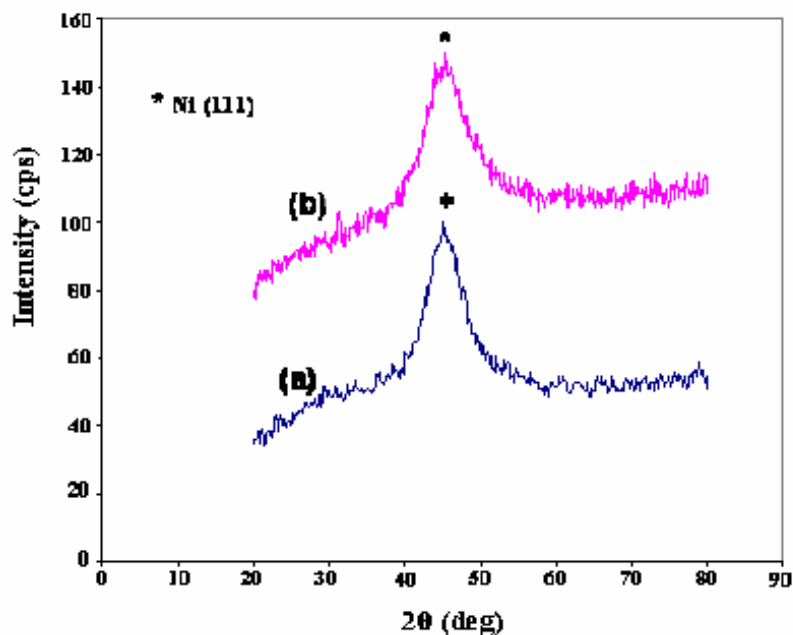
Figure 4. XRD patterns of as-deposited electroless nickel coatings (a) Ni-P; (b) Ni-P-Si$_3$N$_4$

To further confirm the presence of the Si$_3$N$_4$ particles in the coating, EDX analysis of the surface has been carried out and the corresponding spectra is shown in the Figure 5. Silicon peak is observed other than nickel and phosphorous peaks. This confirms the presence of second phase silicon nitride particles in the NiP matrix.
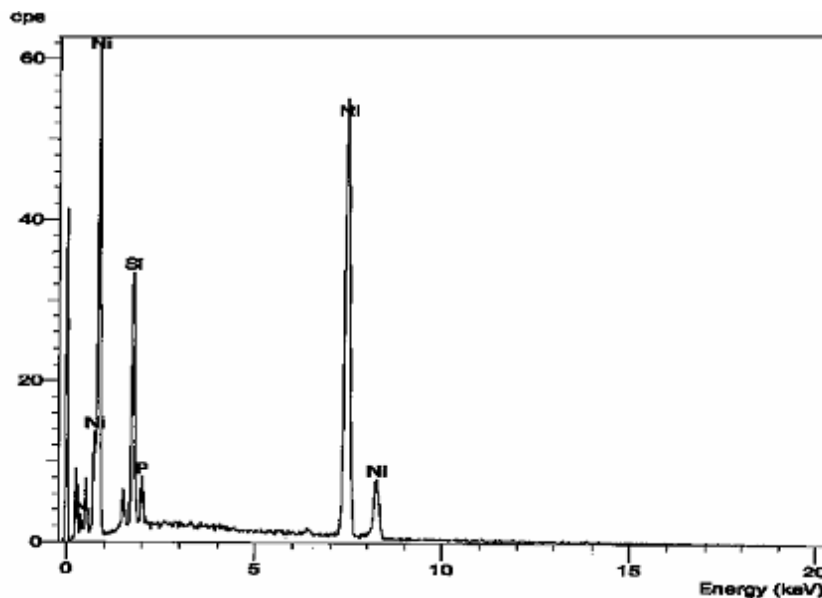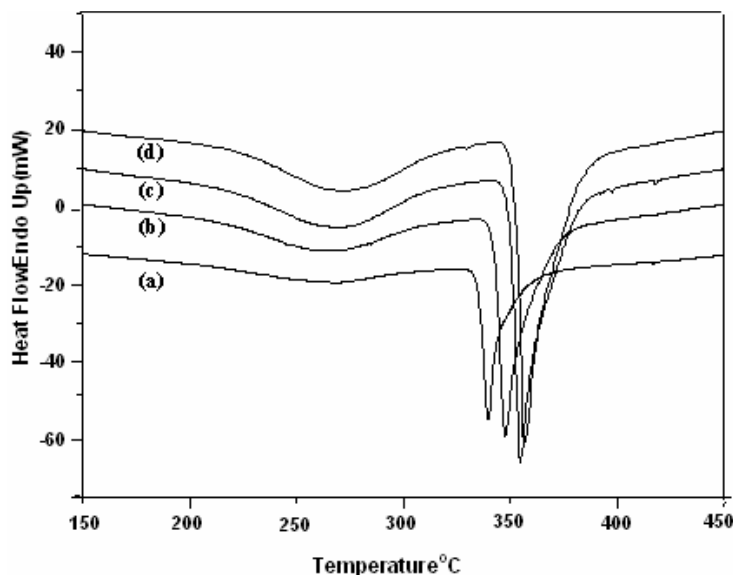

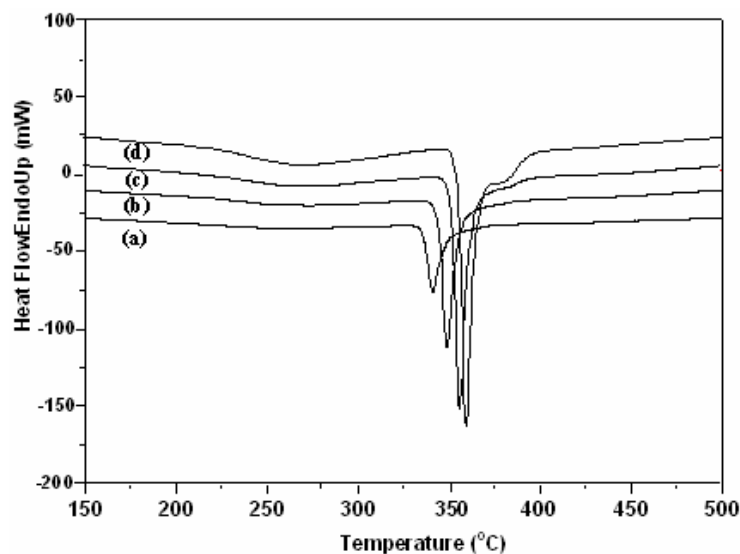**Figure 5.** EDX Spectra of electroless Ni-P-Si$_3$N$_4$ composite coating

3.5. Phase transformation behaviour

Crystallization and phase transformation behavior of electroless nickel coatings plays a vital role in determining the coating properties. Investigations on the electroless Ni-P deposits have shown that different deposit compositions and heat treatment conditions could affect both the microstructural characteristics and crystallization behavior of the deposit.

Figure 6. DSC thermograms of electroless Ni-P coating (a) 10°C/ min.; (b) 20°C/ min.; (c) 30°C/ min.; (d) 40°C/ min.
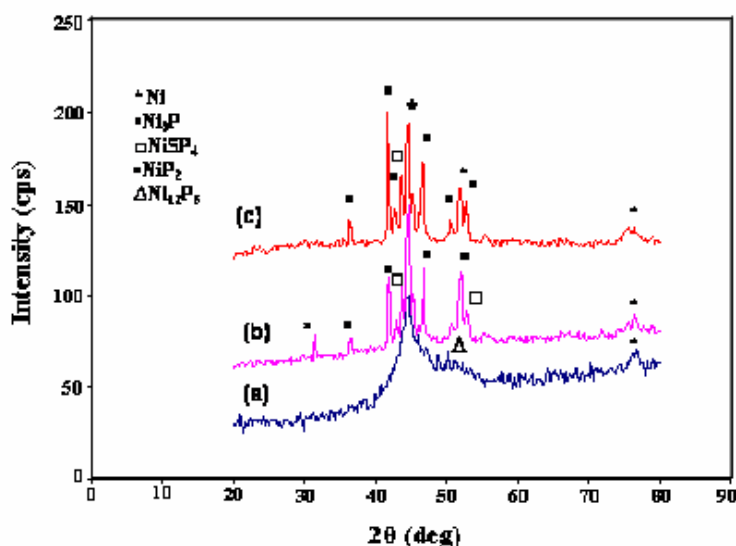

Figure 7. DSC thermograms of electroless Ni-P-Si$_3$N$_4$ coating (a) 10°C/ min.; (b) 20°C/ min.; (c) 30°C/ min.; (d) 40°C/ min.

To understand the phase transformation behavior differential scanning calorimetry (DSC) studies were carried out on the foils of the electroless Ni-P and composite coatings at different

scanning rates of 10, 20, 30, 40°C/ min. in the temperature range of 150-500°C. DSC thermograms obtained for the plain electroless Ni-P and Ni-P-Si$_3$N$_4$ composite coatings are shown in the Figures 6-7. Exothermic peak temperatures and enthalpy values of both the coatings at different scanning rates are given in Table 3. With the increase in the heating rate, the areas of the exothermic peaks increase. It is also evident that the exothermic peaks become sharper and deeper with increase in the heating rate.

Table 3. Peak temperature and ΔH values obtained at different scanning rates

Heating Rate (°C)	Peak temperature (^{o}C) and ΔH (J/ g)			
	P1	ΔH	P2	ΔH
Ni-P				
10	259	-19	340	-47
20	263	-28	347	-45
30	271	-22	354	-43
40	273	-19	356	-34
Ni-P-Si$_3$N$_4$				
10	---	---	341	-50
20	---	---	348	-48
30	---	---	356	-49
40	266	-16	360	-49

Figure 8. XRD graphs of electroless nickel coatings annealed at exothermic peak temperatures (a) Ni-P H.T. at 280°C; (b) Ni-P H.T. at 360°C; (c) Ni-P-Si$_3$N$_4$ H.T at 360°C

Using the modified Kissinger method, activation energies for both the coatings were calculated. In this method a linear regression line has been obtained form the plot of $\ln(T_m^2/\Phi)$ versus $(1000/RT_m)$, using peak temperature (T_m) of crystallization process represented by the major exothermic peak of DSC curve, at different heating rate Φ. The slope of this line yields the activation energy (Q) of the deposit [19]. To find out the phases formed during exothermic reaction at peak temperatures, Ni-P and

composite coatings were annealed at respective peak temperatures. Then the samples were analyzed using XRD method. The XRD patterns obtained are shown in the Figure 8. Phases obtained for all the deposits in the annealed conditions are given in the Table 4.

Table 4. Phase transformation obtained from the XRD data for both electroless Ni-P and composite coatings in as-plated and heat-treated conditions*

Temperature (°C)	Phases present
Ni-P	
R.T	Ni (111) [1.2nm]
280°C	Ni (111) [1.7 nm], Ni (220), $Ni_{12}P_5$ (312)
360°C	Ni (111) [14 nm], Ni (200), Ni (220), Ni_3P (141),
	Ni_3P (112), NiP_2 (130), NiP_2 (002), Ni_5P_4 (204), Ni_5P_4 (214)
Ni-P–Si₃N₄	
R.T.	Ni (111) [1.7nm]
360°C	Ni (111) [21 nm], Ni (200), Ni (220), Ni_3P (231),
	Ni_3P (031), Ni_3P (141), Ni_3P (222), Ni_3P (132),
	NiP_2 (221), NiP_2 (130), Ni_5P_4 (212), Ni_5P_4 (214)

*Grain sizes calculated using Debye- Scherrer method is given in square bracket.

DSC thermograms obtained for the electroless Ni-P coating at different scanning rates is given in the Figure 6. It shows that the presence of a major exothermic peak in the range of 340-400°C at 40°C/ min scanning. In addition, a broad and very shallow peak (225-300°C) is also found right before the major exothermic peak. The formation of a shallow peak at lower temperature region in the DSC curves may be due to the first stage transformation i.e. the short range atomic movements and the incipient crystallization of the metastable crystalline structure [20]. These short range atomic movements include structural relaxation such as annihilation of point defects and dislocations within the grain and grain boundary zones. The major exothermic peak is associated with the long range atomic movements causing the precipitation of stable phases such as f.c.c nickel and b.c.t nickel phosphide phases. The activation energy calculated using the modified Kissinger method for the plain electroless Ni-P coating are 196±2 kJ/mole and 243±7 kJ/ mole for the first and second exothermic peaks respectively. The obtained activation energy value for the major peak was found relatively close to the self-diffusion activation energy of nickel, 289 kJ/ mole [20].

The XRD studies carried out for the plain Ni-P coatings annealed at the first exothermic peak temperature (280°C) exhibits a number of small peaks emerged from the major diffraction peak. These peaks correspond to f.c.c Ni and metastable $Ni_{12}P_5$. Since no stable Ni_3P has formed and only the intensity of amorphous phase decreased, it shows that phase transformation has not yet begun. It can also be noted that the grain size of nickel remains same as that of as-deposited coating approx. 1.7 nm. Keong et al [19] have also observed similar results except that they have not found any $Ni_{12}P_5$ phase at 300°C, but after 350°C annealing $Ni_{12}P_5$ phase was noticed. The XRD result of second exothermic peak (360°C) shows the presence of stable Ni and Ni_3P, metastable NiP_2 and Ni_5P_4 phases. This indicates the ongoing of major crystallization reaction in the deposit. Here the amorphous phase

remains, but further decreased in amount. Apart from that number of low intensity diffraction peaks are present, which are possibly caused by the residual stresses of the deposit [19]. Comparing the grain sizes of as-deposited and low temperature annealed deposits, it can be observed that the grain coarsening has occurred at 360°C. Still Ni (111) peak is the most intense diffraction peak. Thus we can conclude that the phase transformation has not completed yet. Keong et al [20] have reported that the annealing at 800°C completes the phase transformation of Ni-P (10-14 wt.% P) coatings. At this stage only intense peaks of f.c.c Ni and b.c.t Ni_3P are found in the XRD profile of the very high temperature annealed deposit. Hence, in the present study the complete transformation to occur for the metastable nickel phosphides to stable Ni_3P of the electroless nickel coatings, heat treatment at very high temperature is necessary.

The DSC thermograms of electroless Ni-P-Si_3N_4 composite coatings are shown in the Figure 7. From the figure it is evident that the presence of a major exothermic peak in the temperature range of 350-410°C. From the Figure 7 it can also be seen that the presence of a very weak, low temperature peak only in the case of thermogram obtained at 40°C/min. scanning rate. Where as in the case of plain electroless Ni-P coatings the low temperature peak is seen at all scanning rates. From this it can be inferred that probably the composite coating needs high heat input for a short duration to reveal the phase transformation at low temperature. There is a slight increase in the peak temperature can be seen for the composite coating compared to plain electroless Ni-P coating. The additional, a small high temperature peak for the Ni-P-Si_3N_4 composite coating can be seen at around 390°C. The small difference in the peak temperature between first and second peak suggest possible splitting. Splitting of higher temperature peak is generally reported for hypoeutectic Ni-P alloys [21] due to the differences in activation energy for crystallization from partially crystallized matrix and amorphous matrix. Similar observation has been made for the electroless Ni-P-TiO_2 system elsewhere [12]. The calculated activation energy for the composite coating is 224±3 kJ/mol. There is marginal decrease in the activation energy can be noticed for the composite coating compared to that of plain Ni-P coating.

Based on the above it can be inferred that the incorporation of silicon nitride particles do not have much influence on the phase transformation behaviour of electroless Ni-P deposit. This is not surprising as the temperature range involved in the phase transformation of these deposits is of the order 340 – 360°C, the second phase particles will not undergo any modification to cause a major change in the phase transformation behaviour of the deposit. With such an analogy, it is possible to ascertain that even the observed variations in the DSC thermograms of the electroless Ni-P-Si_3N_4 composite coating is not due to the influence of the incorporated second phase silicon nitride particles but believed to be due to the matrix itself.

Phases present at the transformation temperature is identified by XRD studies and are given in the Table 4. They are Ni, Ni_3P, NiP_2 and Ni_5P_4 same as obtained for the particle free coating. This also confirms that particles codeposited do not influence the phase transformation. Gao Jiaqiang et al [16] for SiC particles, Yating Wu et al. [22] for PTFE+SiC particles and Balaraju et al [24] for micron size Si_3N_4, TiO_2 and CeO_2 particles have got similar results. Gao Jiaqiang et al [15] have observed that there is a second exothermic peak at 550°C in the DSC thermogram of the composite Ni-P-SiC coating which corresponds to the reaction between nickel and SiC particles. They have also found that there is a slight decrease in the reaction temperature with the decrease in particle size. But Huang et al [24]

have obtained two exothermic peaks in the DSC curve of Ni-P-PTFE-SiC composite coating. According to them the first peak (280°C) is due to the stress relaxation of the particle matrix interface and second peak (340°C) is associated with the phase transformation from amorphous Ni-P to polycrystalline Ni and Ni$_3$P alloy. In contrast to this Gao Jiaqiang et al [25] have found that the nanometric Al$_2$O$_3$ particle have reduced the crystallization temperature of Ni-P-Al$_2$O$_3$ coating.

3.6. Microhardness

Microhardness measurements were made on the cross-sections of the plain electroless Ni-P and Ni-P-Si$_3$N$_4$ composite coatings in as-plated and heat-treated at various temperatures. Hardness results obtained for both the coatings were given in the Table 5. It is evident from the table that there was nearly 10% increase in the hardness values obtained due to the second phase particle reinforcement in the Ni-P matrix. For both the electroless nickel coatings there was increasing trend in the microhardness values until the heat treatment temperature of 400°C. This increment in hardness is very high at 400°C. About 22% increase in hardness values could be seen for the electroless nickel composite coatings compared to the plain Ni-P. From the Table 5 it could also be seen that at 600°C annealing temperature there was more than 30% reduction in the microhardness values compared to that of 400°C annealed deposits. It was interesting to note that these high temperature heat treated deposits microhardness values were higher than that of the as-deposited coatings.

Table 5. Microhardness values of electroless Ni-P and Ni-P-Si$_3$N$_4$ coatings in as-plated and annealed at various temperatures (200, 400 and 600°C for 1 hour)

Type of coating	Microhardness (VHN$_{50gf}$)			
	As-plated	**200°C**	**400°C**	**600°C**
Ni-P	600	630	980	640
Ni-P-Si$_3$N$_4$	655	695	1220	735

In general, the heat treatment process transforms the Ni-P phase to a mixture of hard nickel phosphides (Ni$_3$P) and nickel. From the EDX values given in the Table 2 it is evident that the amount of phosphorus present in both the coatings are about 10 wt.%. Hence, higher is the phosphorus content in the deposit; higher is the nickel phosphides formation due to the heat treatment at 400°C temperature. This transformation is the main reason for increase in hardness with heat treatment. It is known from the theory of hardening of materials that when a fine precipitate is formed in a solid solution; an additional barrier is formed for the movement of dislocation to propagate. It is generally believed that these dislocations cut through the precipitate particle till they are coherent to the matrix. Apart from this dispersion strengthening due to the second phase silicon nitride particles also influences the improvement in microhardness in the case of composite coatings. This can be clearly seen in Table 5 where the microhardness values obtained for plain Ni-P and composite coatings at 400°C annealing treatment are 980 and 1220 VHN respectively. But as the heat treatment temperature increases, above 400°C, the finely dispersed crystallites of Ni$_3$P and Ni agglomerates (grain coarsening) and they become incoherent to the matrix. Hence, it becomes easier for a dislocation to

loop between these coarse particles rather than to shear them. This is the reason for decrease in the hardness of coatings after 400°C. Similar results are reported in the literature [25-27].

The above studies on the preparation and characterization of hypophosphite reduced nickel composite coatings show that the incorporation of silicon nitride particles influences the morphology of the deposit. Deposit exhibits more nodular morphology due to the particles incorporation. Composition, structure and crystallization temperature of the deposit is not influenced much by the codeposition of these second phase particles. Annealed composite deposit at crystallization temperature indicated that phase transformation is not complete and the metastable phases like NiP_2 and Ni_5P_4 are present. Higher microhardness values can be obtained at 400°C annealed deposits due to the codeposition of silicon nitride particles.

4. CONCLUSIONS

Electroless Ni-P composite coatings containing submicron silicon nitride particles were successfully prepared using a hypophosphite reduced bath. EDX analysis carried out on the surface and cross-sectional deposits of both coatings revealed that there was almost no variation in the phosphorus content codeposited. Plain electroless Ni-P deposits seem to be smooth compared to the slightly nodular deposits obtained due to the particle reinforcement. Particle codeposition was uniform through out the cross-section of the composite coating. XRD and DSC results obtained for the both coatings revealed that particles did not influence the structure and phase transformation behaviour. Presence of metastable phases was identified for the deposits annealed at crystallization temperature. Higher microhardness values obtained for composite coatings in as-plated and at all heat-treated conditions were due to the silicon nitride particles incorporation.

References

1. G.O. Mallory, J.B. Hajdu, Electroless Plating: Fundamentals and Applications, AESF, Orlando, 1991.
2. Metzger, Th Florian, *Trans. Inst. Met. Finish.* 54 (1976) 174.
3. S.S. Tulsi, *Finishing* 7(11) (1983) 14.
4. J. Lukschandel, *Trans. Inst. Met. Finish.* 56(3) (1978) 118.
5. Z. Abdel Hamid, S.A. El Badry, A. Abdel Aal, *Surf. Coat. Technol.* 201(2007) 5948.
6. J. Novakovic, P. Vassiliou, Kl. Samara, Th. Argyropoulos *Surf. Coat. Technol.* 201(3-4) (2006) 895.
7. M. Sarret, C. Muller, A. Amell, *Surf. Coat. Tech.* 201 (1-2) (2006) 389.

8. I. Apachitei, F.D. Tichelaar, J. Duszczyk, L. Katgerman, *Surf. Coat. Technol*. 149 (2002) 263.
9. C.M. Das, P.K. Limaye, A.K. Grover, A.K. Suri, *J. Alloys Compd*. Article in press.
10. J.N. Balaraju, Kalavathy, K.S. Rajam, *Surf. Coat. Technol*. 200 (2006) 3933
11. Xinguo, H and L Naichao, In Proc. Asia Pacific Int. Finish.'90, The Australian Institute of Metal Finishing, Melbourne, (1990) 26.1-26.9.
12. J.N. Balaraju, PhD Thesis, I.I.T. Madras, Chennai (2000).
13. L. Brown, *Trans. Inst. Met. Fin*. 63 (1985)139.
14. Wu Yucheng, Li Guanghai, Zhang Lide, Yan Bo, Z. Metallkd. 91(9) (2000) 788.
15. Gao Jiaqiang, Liu Lei, Wu Yating, Shen Bin, Hu Wenbin, *Surf. Coat. Technol*. 200 (20-21) (2006) 5836.
16. K.G. Keong, W. Sha, *Surf. Engg*. 8(5) (2002) 329.
17. J.N. Balaraju, T.S.N. Sankara Narayanan, S.K. Seshadri, *J. App. Electrochem*., 33 (2003) 807.
18. I. Apachitei, F.D. Tichelaar, J. Duszczyk, L. Katgerman, *Surf. Coat. Technol*. 149 (2002) 263.
19. K.G. Keong, W. Sha, S. Malinov, *Acta Metall. Sin*. 14(6) (2001) 419.
20. K.G. Keong, W. Sha, S. Malinov, *J. Alloys. Compd*. 334 (2002) 192.
21. K.S. Rajam, I. Rajagopal, S.R. Rajagopalan, B. Viswanathan, Mater. *Chem. Phys*. 33 (1993) 289.
22. Yating Wu, Lei Liu, Bin Shen, Wenbin Hu, *J. Mat. Sci*. 40(18) (2005) 5057.
23. J.N. Balaraju, T.S.N. Sankara Narayanan, S.K. Seshadri, *Mat. Res. Bull*. 41 (2006) 847.
24. Y.S. Huang, X.T. Zeng, I. Annergren, F.M. Liu, *Surf. Coat. Technol*.167 (2003), 207.
25. Gao Jiaqiang, Wu Yating, Liu Lei, Hu Wenbin, *Mat. Lett*. 59 (2005) 391.
26. M.H. Staia, A. Conzono, M.R. Cruz, A. Roman, J. Lesage, D. Chicot, G. Mesmacque, *Surf. Engg*. 18 (4) (2002) 265.
27. X. Huang, Y. Wu, L. Qian, *Plat. Surf. Fin*. 91 (2004) 46.